

# *Homo sapiens* in Arabia by 85,000 years ago

Huw S. Groucutt<sup>1,2\*</sup>, Rainer Grün<sup>3,4</sup>, Iyad S.A. Zalmout<sup>5</sup>, Nick A. Drake<sup>6</sup>, Simon J. Armitage<sup>7,8</sup>, Ian Candy<sup>7</sup>, Richard Clark-Wilson<sup>7</sup>, Julien Louys<sup>3</sup>, Paul S. Breeze<sup>6</sup>, Mathieu Duval<sup>3,9</sup>, Laura T. Buck<sup>10,11</sup>, Tracy L. Kivell<sup>12,13</sup>, Emma Pomeroy<sup>10,14</sup>, Nicholas B. Stephens<sup>13</sup>, Jay T. Stock<sup>10,15</sup>, Mathew Stewart<sup>16</sup>, Gilbert J. Price<sup>17</sup>, Leslie Kinsley<sup>4</sup>, Wing Wai Sung<sup>18</sup>, Abdullah Alsharekh<sup>19</sup>, Abdulaziz Al-Omari<sup>20</sup>, Muhammad Zahir<sup>21</sup>, Abdullah M. Memesh<sup>5</sup>, Ammar J. Abdulshakoor<sup>5</sup>, Abdu M. Al-Masari<sup>5</sup>, Ahmed A. Bahameem<sup>5</sup>, Khaled S.M. Al Murayyi<sup>20</sup>, Badr Zahrani<sup>20</sup>, Eleanor M.L. Scerri<sup>1,2</sup> & Michael D. Petraglia<sup>2,22\*</sup>

<sup>1</sup> School of Archaeology, Research Laboratory for Archaeology and the History of Art, Hayes House, 75 George Street, University of Oxford, Oxford, OX1 2BQ, UK.

<sup>2</sup> Department of Archaeology, Max Planck Institute for the Science of Human History, Kahlaische Stasse 10, D-07743, Jena, Germany.

<sup>3</sup> Australian Research Centre for Human Evolution (ARCHE), Environmental Futures Research Institute, Griffith University, Nathan, QLD 4111, Australia.

<sup>4</sup> Research School of Earth Sciences, The Australian National University, Canberra ACT, 0200, Australia.

<sup>5</sup> Saudi Geological Survey, Sedimentary Rocks and Palaeontology Department, Jeddah 21514, Saudi Arabia.

<sup>6</sup> Department of Geography, King's College London, Strand, London WC2R 2LS, UK

<sup>7</sup> Department of Geography, Royal Holloway, University of London, TW20 0EX UK

<sup>8</sup> SFF Centre for Early Sapiens Behaviour (SapienCE), University of Bergen, Post Box 7805, 5020, Bergen, Norway.

<sup>9</sup> Geochronology, Centro Nacional de Investigación sobre la Evolución (CENIEH), Paseo Sierra de Atapuerca, 3, 09002 Burgos, Spain

- 27 <sup>10</sup> PAVE Research Group, Dept. of Archaeology, University of Cambridge, Cambridge, CB2 3QG,  
28 UK.
- 29 <sup>11</sup> Earth Sciences Department, Natural History Museum, Cromwell Road, London, SW7 5BD, UK.
- 30 <sup>12</sup> Skeletal Biology Research Centre, School of Anthropology and Conservation, University of Kent,  
31 Canterbury, CT2 7NR, UK.
- 32 <sup>13</sup> Department of Human Evolution, Max Planck Institute for Evolutionary Anthropology, Deutscher  
33 Platz 6, 04103, Leipzig, Germany.
- 34 <sup>14</sup> School of Natural Sciences and Psychology, Liverpool John Moores University, Liverpool, L3 3AF,  
35 UK.
- 36 <sup>15</sup> Department of Anthropology, University of Western Ontario, London, Ontario, N6A 3K7, Canada.
- 37 <sup>16</sup> Palaeontology, Geobiology and Earth Archives Research Centre, School of Biological, Earth and  
38 Environmental Science, University of New South Wales, Sydney 2052, Australia.
- 39 <sup>17</sup> School of Earth and Environmental Sciences, The University of Queensland, St Lucia 4072,  
40 Queensland, Australia.
- 41 <sup>18</sup> Department of Life Sciences, The Natural History Museum, Cromwell Road, London SW7 5BD,  
42 UK.
- 43 <sup>19</sup> Department of Archaeology, King Saud University, Riyadh, 12372 Saudi Arabia.
- 44 <sup>20</sup> Saudi Commission for Tourism and National Heritage, Riyadh 11586, Saudi Arabia.
- 45 <sup>21</sup> Department of Archaeology, Hazara University, Mansehra, 21300, Pakistan.
- 46 <sup>22</sup> Human Origins Program, National Museum of Natural History, Smithsonian Institution,  
47 Washington, DC, 20560, USA.

48

49 Corresponding authors: HSG (huw.groucutt@rlaha.ox.ac.uk) and MDP (petraglia@shh.mpg.de)

50

51

52

53 Understanding the timing and character of *Homo sapiens* expansion out of Africa is critical  
54 for inferring the colonisation and admixture processes that underpin global population  
55 history. It has been argued that dispersal out of Africa had an early phase, particularly ~130-  
56 90 thousand years ago (ka), that only reached the East Mediterranean Levant, and a later  
57 phase, ~60-50 ka, that extended across the diverse environments of Eurasia to Sahul.  
58 However, recent findings from East Asia and Sahul challenge this model. Here we show that  
59 *H. sapiens* was in the Arabian Peninsula before 85 ka. We describe the Al Wusta-1 (AW-1)  
60 intermediate phalanx from the site of Al Wusta in the Nefud Desert, Saudi Arabia. AW-1 is  
61 the oldest directly dated fossil of our species outside Africa and the Levant. The  
62 palaeoenvironmental context of Al Wusta demonstrates that *H. sapiens* using Middle  
63 Palaeolithic stone tools dispersed into Arabia during a phase of increased precipitation driven  
64 by orbital forcing, in association with a primarily African fauna. A Bayesian model  
65 incorporating independent chronometric age estimates indicates a chronology for Al Wusta of  
66 ~95-86 ka, which we correlate with a humid episode in the later part of Marine Isotope Stage  
67 5 known from various regional records. Al Wusta shows that early dispersals were more  
68 spatially and temporally extensive than previously thought. Early *H. sapiens* dispersals out of  
69 Africa were not limited to winter rainfall-fed Levantine Mediterranean woodlands  
70 immediately adjacent to Africa, but extended deep into the semi-arid grasslands of Arabia,  
71 facilitated by periods of enhanced monsoonal rainfall.

72

### 73 **Background**

74

75 *Homo sapiens* evolved in Africa in the late Middle Pleistocene<sup>1</sup>. Early dispersals out of  
76 Africa are evidenced at the Levantine site of Misliya at ~194-177 ka<sup>2</sup>, followed by Skhul and  
77 Qafzeh, where *H. sapiens* fossils have been dated to ~130-100 and ~100-90 ka respectively<sup>3</sup>.

78 While the Levantine fossil evidence has been viewed as the onset of a much broader dispersal  
79 into Asia<sup>4-6</sup>, it has generally been seen as representing short-lived incursions into the  
80 woodlands of the Levant immediately adjacent to Africa, where relatively high precipitation  
81 is produced by winter storms tracking across the Mediterranean<sup>7,8</sup>. While the Levantine  
82 record indicates the subsequent local replacement of early *H. sapiens* by Neanderthals, the  
83 failure of early dispersals to extend beyond the Levant is largely inferred from interpretations  
84 of genetic data<sup>9</sup>. Genetic studies have suggested that recent non-African populations stem  
85 largely<sup>10</sup>, if not entirely<sup>9</sup>, from an expansion ~60-50 ka, but this model remains debated. The  
86 absence of low latitude Pleistocene human DNA and uncertainties regarding ancient  
87 population structure undermine conclusions drawn from genetic studies alone. The paucity of  
88 securely dated archaeological, palaeontological and ancient DNA data - particularly across  
89 southern Asia - has made testing dispersal hypotheses challenging<sup>4,7,11</sup>.

90

91 Recent fossil discoveries in East Asia indicate that the early (particularly Marine Isotope  
92 Stage 5) dispersals of *Homo sapiens* extended across much of southern Asia. At Tam Pa Ling  
93 in Laos, *Homo sapiens* fossils date to between 70 and 46 ka<sup>12</sup>. Teeth assigned to *Homo*  
94 *sapiens* from Lida Ajer cave, Sumatra, were recovered from a breccia dating to  $68 \pm 5$  ka,  
95 with fauna from the site dating to  $75 \pm 5$  ka<sup>13</sup>. Several sites in China have produced fossil  
96 material claimed to represent early *Homo sapiens*<sup>14</sup>. These include teeth from Fuyan Cave  
97 argued to be older than 80 ka based on the dating of an overlying speleothem a few metres  
98 from the fossils<sup>15</sup>, and teeth from Luna Cave that were found in a layer dating to between  
99  $129.9 \pm 1.5$  ka and  $70.2 \pm 1.4$  ka<sup>16</sup>. Teeth and a mandible from Zhiren Cave, China, date to at  
100 least 100 ka and have been argued to represent *Homo sapiens*, but other species attributions  
101 are possible<sup>17</sup>. The recent documentation of a human presence in Australia from ~65 ka is  
102 consistent with these findings<sup>18</sup>. Likewise, some interpretations of genetic data are consistent

103 with an early spread of *Homo sapiens* across southern Asia<sup>10</sup>. These discoveries are leading  
104 to a radical revision of our understanding of the dispersal of *Homo sapiens*, yet there remain  
105 stratigraphic and taxonomic uncertainties for many of the east Asian fossils<sup>14,19</sup>, and  
106 thousands of kilometers separate these findings from Africa.

107

108 The Arabian Peninsula is a vast landmass at the crossroads of Africa and Eurasia. Growing  
109 archaeological evidence demonstrates repeated hominin occupations of Arabia<sup>20,21</sup> each  
110 associated with a strengthened summer monsoon which led to the re-activation of lakes and  
111 rivers<sup>22-24</sup>, as it did in North Africa<sup>25</sup>. Here we report the discovery of the first pre-Holocene  
112 human fossil in Arabia, Al Wusta-1 (AW-1), as well as the age, stratigraphy, vertebrate  
113 fossils and stone tools at the Al Wusta site (Fig. 1, see also Supplementary Information).

114

115 **\*Figure 1 hereabouts\***

116

## 117 **Results**

118 AW-1 is an intermediate manual phalanx, most likely from the 3<sup>rd</sup> ray (Fig. 2a,  
119 Supplementary Information 1: see below for detail on siding and species identification). It is  
120 generally well-preserved, although there is some erosion of the cortical/subchondral bone,  
121 and minor pathological bone formation (likely an enthesophyte) affecting part of the  
122 diaphysis (Supplementary Information 1). The phalanx measures 32.3 mm in proximo-distal  
123 length, and 8.7 mm and 8.5mm in radio-ulnar breadth of the proximal base and midshaft,  
124 respectively (Supplementary Table 1).

125

126 AW-1 is more gracile than the robust intermediate phalanges of Neanderthals<sup>26-28</sup>, which are  
127 broader radio-ulnarly relative to their length and have a more 'flared' base. AW-1's proximal

128 radio-ulnar maximum breadth is 14.98 mm, which provides an intermediate phalanx breadth-  
129 length index (proximal radio-ulnar maximum breadth relative to articular length) of 49.6.  
130 This is very similar to the mean ( $\pm$  SD) for the Skhul and Qafzeh *H. sapiens* of 49.7 ( $\pm$  4.1)  
131 and 49.1 ( $\pm$  4.0) for Upper Palaeolithic Europeans, but 1.89 standard deviations below the  
132 Neanderthal mean of 58.3 ( $\pm$  4.6)<sup>29</sup>.

133

134 **\*Figure 2 hereabouts\***

135

136 To provide a broad interpretive context for the Al Wusta phalanx, we conducted linear and  
137 geometric morphometric (GMM) landmark analyses (Supplementary Information 1) on  
138 phalanges from non-human primates, fossil hominins and geographically widespread recent  
139 *H. sapiens*. Comparative linear analyses (Supplementary Information 1, Supplementary  
140 Tables 2 and 3, Supplementary Figure 1) reveal that there is substantial overlap across most  
141 taxa for all shape ratios, so AW-1 falls within the range of variation of *H. sapiens*, cercopiths,  
142 *Gorilla*, *Australopithecus afarensis*, *A. sediba* and Neanderthals. However, AW-1 is most  
143 similar to the median value or falls within the range of variation of recent and early *H.*  
144 *sapiens* for all shape ratios.

145

146 Geometric morphometric (GMM) analyses of AW-1 and various primate groups including  
147 hominins (see Supplementary Table 4 and Supplementary Figure 2 for landmarks, and  
148 Supplementary Table 5 for sample) are illustrated in Figure 3 and Supplementary Figure 3.  
149 PC1 and PC2 together account for 61% of group variance in shape. AW-1 is separated on  
150 these two shape vectors from the non-human primates and most of the Neanderthals. AW-1  
151 falls closest to the recent and early *H. sapiens* and is clearly differentiated from all non-

152 human primates. This is also shown by the Procrustes distances from AW-1 to the mean  
153 shapes of each taxonomic group (Supplementary Table 6).

154

155 **\*Figure 3 hereabouts\***

156

157 Three of the Neanderthal phalanges (from Kebara 2 and Tabun C1) are quite disparate from  
158 the main Neanderthal cluster and fall closer to the *H. sapiens* and Al Wusta cluster on PC1  
159 and 2 (Figure 3 and Supplementary Figure 3). Having established the hominin affinity of  
160 AW-1, shape was analysed in more detail using a smaller hominin sample for which ray  
161 number and side were known, which included Kebara 2 and Tabun C1. The broader primate  
162 sample used in the first GMM analysis was not used for the more detailed shape analysis, as  
163 the initial comparisons show clearly that AW-1 is not a non-human primate and including  
164 this level of variation could potentially mask more subtle shape differences between  
165 hominins. The side and ray are also not known for most of the Neanderthal and non-human  
166 primate samples, meaning it would be impossible to evaluate the effect of these factors using  
167 this sample.

168

169 The more in-depth shape comparison and modelling using the hominin sample of phalanges  
170 of known ray and side (Supplementary Table 7) demonstrates that the long and slender  
171 morphology of AW-1 falls just outside the range of variation of comparative Middle  
172 Palaeolithic modern humans, but that its affinity is clearly with *H. sapiens* rather than  
173 Neanderthals (Fig. 4, Supplementary Table 8). Although both Pleistocene *H. sapiens* and  
174 Neanderthal landmark configurations fall almost completely inside the scatter for the  
175 Holocene *H. sapiens* sample in the principal components analysis (Figure 4), AW-1 is closest  
176 to Holocene *H. sapiens* 3<sup>rd</sup> intermediate phalanges. AW-1 overlaps with the Holocene *H.*

177 *sapiens* sample, but is separated from the Pleistocene *H. sapiens* specimens by a higher score  
178 on PC2 and from the Neanderthal group by a simultaneously higher score on PC1 and PC2.  
179 The Procrustes distances (Supplementary Table 8), also show that AW-1 is most distinct  
180 from the Neanderthal phalanges, which fall towards the lower ends of both PCs and are  
181 characterised by shorter and broader dimensions. PC1 and PC2 in this analysis show that  
182 AW-1 is taller and narrower (in all directions: dorso-palmarly, proximo-distally and radio-  
183 ulnarly) than almost all the phalanges in the comparative sample and is particularly distinct  
184 from most of the Neanderthal phalanges. In this analysis AW-1 is closest in shape to 3<sup>rd</sup>  
185 phalanges of individuals from (in descending order of proximity) Egyptian Nubia, and  
186 Medieval Canterbury (UK), and Maiden Castle (Iron Age Dorset, UK) (Supplementary Table  
187 9), although there is not a great difference in its distance to any of these specimens. These  
188 analyses suggest that the AW-1 phalanx is likely to be a 3<sup>rd</sup> intermediate phalanx from a *H.*  
189 *sapiens* individual.

190

191 **\*Figure 4 hereabouts\***

192

193 The third ray is the most symmetrical ray in the hand and is therefore difficult to side,  
194 particularly when not all of the phalanges of a particular individual are present. Comparing  
195 AW-1 separately to right and to left phalanges (Supplementary Information 1.4) gives results  
196 which are very similar to the pooled sample, such that AW-1 is closest to Holocene *H.*  
197 *sapiens* 3<sup>rd</sup> rays for both right and left hands (Supplementary Figure 4, Supplementary Table  
198 10). There is little difference in morphological closeness between AW-1 and its nearest  
199 neighbour in the samples of right and left bones (Supplementary Table 11), reflecting the lack  
200 of difference in morphology between the sides. It is therefore not possible to suggest whether  
201 AW-1 comes from a right or a left hand using these analyses.



202

203 AW-1 is unusual in its more circular midshaft cross-sectional shape (Fig. 2B), which is  
204 confirmed by cross-sectional geometric analyses (Supplementary Information 1.5). This may  
205 reflect the pronounced palmar median bar that makes the palmar surface slightly convex at  
206 the midshaft rather than flat, the latter being typical of most later *Homo* intermediate  
207 phalanges. However, more circular shafts may reflect greater loading of the bone in multiple  
208 directions and enthesophytes are a common response to stress from high levels of physical  
209 activity<sup>30</sup>. This morphology may reflect high and varied loading of the fingers during intense  
210 manual activity.

211

212 To determine the age of AW-1, and associated sediments and fossils, we used a combination  
213 of uranium series (U-series), electron spin resonance (ESR) and optically stimulated  
214 luminescence (OSL) dating (Methods, Supplementary Information 2 and 3). U-series ages  
215 were produced for AW-1 itself ( $87.6 \pm 2.5$  ka) and hippopotamus dental tissues (WU1601),  
216 which yielded ages of  $83.5 \pm 8.1$  ka (enamel) and  $65.0 \pm 2.1$  ka (dentine). They should be  
217 regarded as minimum estimates for the age of the fossils. In addition, a combined U-series-  
218 ESR age calculation for WU1601 yielded an age of  $103 +10/-9$  ka. AW-1 was found on an  
219 exposure of Unit 3b, and WU1601 excavated from Unit 3a, one metre away (Fig 1b). Unit 1  
220 yielded OSL ages of  $85.3 \pm 5.6$  ka (PD17),  $92.2 \pm 6.8$  ka (PD41) and  $92.0 \pm 6.3$  ka (PD15),  
221 while Unit 3a yielded an OSL age of  $98.6 \pm 7.0$  ka (PD40). The OSL age estimates agree  
222 within error with the US-ESR age obtained for WU-1601 and the minimum age of  $\sim 88$  ka  
223 obtained for AW-1. These data were incorporated into a Bayesian sequential phase model<sup>31</sup>  
224 which indicates that deposition of Unit 1 ceased  $93.1 \pm 2.6$  ka (Phase 1: PD15, 17, 41) and  
225 that Units 2 and 3 and all associated fossils were deposited between  $92.2 \pm 2.6$  ka and  $90.4 \pm$   
226  $3.9$  ka (Phase 2: all other ages) (Supplementary Information 4, Supplementary Figure 11).

227

228 This ~95-86 ka timeframe is slightly earlier than most other records of increased humidity in  
229 the region in late MIS 5<sup>32,33</sup>, which correlate with a strengthened summer monsoon  
230 associated with an insolation peak at 84 ka (Fig. 6). The underlying (Unit 3) aeolian sand  
231 layer at Al Wusta correlates with an insolation minimum at the end of MIS 5c. The  
232 chronometric age estimates for the site suggest that lake formation and the associated fauna  
233 and human occupation occurred shortly after this in time. Regional indications of increased  
234 humidity around the 84 ka insolation peak include speleothem formation at ~88 ka in the  
235 Negev<sup>34</sup>, and the formation of sapropel S3 beginning ~86 ka<sup>35</sup>. In both the Levant and  
236 Arabia, records are consistent with this switch from aridity to humidity around this time<sup>32-40</sup>.  
237 Precisely reconstructing regional palaeoclimate at this time and relating it to human  
238 demographic and behavioural change has proved challenging. This reflects both rapid  
239 changes in climate, as well as the complexities involved in dating relevant deposits<sup>41</sup>. In  
240 summary, combining chronological data (Supplementary sections 2-4), interpretation of the  
241 sedimentary sequence (described below), and the regional setting of Al Wusta, we conclude  
242 that lake formation and associated finds such as the AW-1 phalanx relate to the late MIS 5  
243 humid period associated with the 84 ka insolation peak.

244

245 The sedimentary sequence at Al Wusta consists of a basin-like deposit of exposed carbonate-  
246 rich sediments (Unit 2, 0.4-0.8 m thick), underlain by wind-blown sand (Unit 1) and overlain  
247 by water-lain sands (Unit 3). The carbonate rich sediments of Unit 2 are interpreted as  
248 lacustrine marl deposits on the basis of their sedimentology, geochemistry, and diatom  
249 palaeoecology (Figure 1c, Methods, Supplementary Information 5). At both the macro- and  
250 micro-scale, these beds are relatively massive and comprise fine-grained calcite, typical of  
251 material precipitating and accumulating in a still-water lacustrine environment<sup>42</sup>. At the

252 micro-scale there is no evidence for the desiccation or fluctuation of water levels typical of  
253 palustrine/wetland environments<sup>42</sup>, implying that the lake body was perennial. The diatom  
254 flora support this, containing species such as *Aulacoseira italica* and *Aulacoseira granulata*  
255 throughout the sequences, indicating an alkaline lake a few metres deep. The water was fresh,  
256 not saline or brackish, since saline tolerant species and evaporitic minerals are absent  
257 throughout. While  $\delta^{18}\text{O}$  and  $\delta^{13}\text{C}$  values of continental carbonates are controlled by a wide-  
258 range of variables, the values derived from the Al Wusta marl beds are compatible with the  
259 suggestion of marls precipitated in a perennial lake basin. The Al Wusta carbonate beds  
260 therefore indicate a perennial lake body a few metres in depth. The existence of a marl  
261 precipitating lake basin implies that this system was groundwater fed (to allow for sufficient  
262 dissolved mineral material to be present in the lake waters). Although the Al Wusta sequence  
263 represents a single lake basin, the development of such a feature over highly permeable  
264 aeolian sands in a region where no lake systems exist at the present day implies a local  
265 increase in water table that would require an increase in mean annual rainfall. Consequently,  
266 the Al Wusta sequence represents the occurrence of a humid interval at this time. The Unit 2  
267 marl is overlain by a medium-coarse sand (Unit 3) with crude horizontal laminations,  
268 occasional clasts, fragments of ripped up marl and shells of *Melanoides tuberculata* and  
269 *Planorbis* sp. While some vertebrate fossils and lithics were found in the upper part of Unit 2,  
270 most were found in or on the surface of Unit 3. Unit 3a sands are waterlain and represent the  
271 encroachment of fluvial sediment as the lake environment shallowed and contracted. Unit 3b  
272 represents a winnowed lag formed by aeolian deflation of 3a. The sequence is capped by a  
273 dense network of calcitic rhizoliths marking the onset of fully terrestrial conditions.  
274  
275 A total of 860 vertebrate fossils were excavated from Unit 3 and the top of Unit 2 (n=371)  
276 and systematically surface collected (n=489). These include specimens attributed to Reptilia,

277 Aves, and Mammalia (Supplementary Table 19, Methods, Supplementary Information 6).  
278 Notable taxa now extinct in Arabia are predominately grazers and include *Hippopotamus*,  
279 *Pelorovis*, and *Kobus*. The faunal community demonstrates a clear preference for temperate  
280 to semi-arid grasslands, and the presence of *Hippopotamus* and *Kobus* indicate permanent  
281 muddy, fluvial, or lacustrine conditions<sup>43</sup> not currently found in the Nefud Desert, but  
282 consistent with the geological evidence from the site. The faunal assemblages show a strong  
283 affinity to African fauna, particularly *Hippopotamus*, *Pelorovis*, and *Kobus*<sup>44</sup>. Many large  
284 tooth pits on fossils indicate that large carnivores played a role in the accumulation of the  
285 deposit. Long bone circumference, completeness and numbers of green fractures suggests  
286 modification of bones by bone-breaking agents such as large carnivores or hominins  
287 (Supplementary Information 6). However, no evidence of cut-marks or hammerstone damage  
288 to the bones was observed.

289

290 An assemblage of 380 lithic artefacts (stone tools) was recovered from the excavation of  
291 upper Unit 2 and Unit 3 and systematic surface collection (Methods, Figure 5, Supplementary  
292 Information 7). They are of Middle Palaeolithic character and most are chert and quartzite.  
293 The assemblage demonstrates a focus on centripetal Levallois reduction, and is similar to  
294 other late Marine Isotope Stage 5 assemblages in the west and north of Arabia<sup>45</sup>, and  
295 contemporaneous assemblages in east (e.g. Aduma, BNS at Omo Kibish) and northeast  
296 Africa (e.g. Bir Tarfawi), as well as those from the Levant (e.g. Qafzeh)<sup>11</sup> (Fig. 5).

297

298 **\*Figure 5 hereabouts\***

299 **\*Figure 6 hereabouts\***

300

301

## 302 **Discussion**

303

304 Al Wusta-1 is the oldest directly dated *H. sapiens* fossil outside Africa and the Levant. It  
305 joins a small but growing corpus of evidence that the early dispersal of *H. sapiens* into  
306 Eurasia was much more widespread than previously thought. The site of Al Wusta is located  
307 in the Nefud desert more than 650 km southeast of Skhul and Qafzeh (Fig. 1A). This site  
308 establishes that *H. sapiens* were in Arabia in late MIS 5, rather than being restricted to Africa  
309 and the Levant as suggested by traditional models (Fig. 6). With Skhul dating to ~130-100  
310 ka, Qafzeh to ~100-90 ka<sup>3,46</sup> and Al Wusta to ~95-85 ka it is currently unclear if the  
311 southwest Asian record reflects multiple early dispersals out of Africa or a long occupation  
312 during MIS 5. The association of the Al Wusta site with a late MIS 5 humid phase (Fig. 6),  
313 suggests that significant aspects of this dispersal process were facilitated by enhanced  
314 monsoonal rainfall. While changes in behaviour and demography are crucial to understanding  
315 the dispersal process, climatic windows of opportunity were also key in allowing *H. sapiens*  
316 to cross the Saharo-Arabian arid belt, which often constituted a formidable barrier<sup>24,25</sup>.

317

## 318 **Conclusion**

319

320 Al Wusta shows that the early, Marine Isotope Stage 5, dispersals of *H. sapiens* out of Africa  
321 were not limited to the Levantine woodlands sustained by winter rainfall, but extended deep  
322 into the Arabian interior where enhanced summer rainfall created semi-arid grasslands  
323 containing abundant fauna and perennial lakes. After long being isolated in Africa<sup>1,47,48</sup>, the  
324 Late Pleistocene saw the expansion of our species out of Africa and into the diverse ecologies  
325 of Eurasia. Within a few thousand years of spreading into Eurasia our species was occupying  
326 rainforest environments and making long sea crossings to remote islands<sup>13,18</sup>. Adapting to the

327 semi-arid conditions of the Saharo-Arabian arid belt represented a crucial step on this  
328 pathway to global success and the Al Wusta *Homo sapiens* fossil demonstrates this early  
329 ability to occupy diverse ecologies which led to us becoming a cosmopolitan species.

330

### 331 **References**

332

- 333 1. Stringer, C. The origin and evolution of *Homo sapiens*. *Philos. Trans. R. Soc. B. Biol.*  
334 *Sci.* **371**, 20150237-20150237 (2016).
- 335 2. Hershkovitz, I., *et al.* The earliest modern humans outside Africa. *Science* **359**, 456-  
336 459 (2018).
- 337 3. Grün, R. *et al.* U-series and ESR analyses of bones and teeth relating to the human  
338 burials from Skhul. *J. Hum Evol.* **49**, 316-334 (2005).
- 339 4. Groucutt, H. S. *et al.* Rethinking the dispersal of *Homo sapiens* out of Africa. *Evol.*  
340 *Anthropol.* **24**, 149-164 (2015).
- 341 5. Petraglia, M. D. *et al.* Middle Paleolithic assemblages from the Indian subcontinent  
342 before and after the Toba super-eruption. *Science* **317**, 114-116 (2007).
- 343 6. Bae, C.J., Douka, K., Petraglia, M.D. On the origin of modern humans: Asian  
344 perspectives. *Science* **358**, DOI: 10.1126/science.aai9067 (2017).
- 345 7. Mellars, P., Gori, K. C., Carr, M., Soares, P. A. & Richards, M. B. Genetic and  
346 archaeological perspectives on the initial modern human colonization of southern  
347 Asia. *Proc. Natl Acad. Sci. USA* **110**, 10699–10704 (2013).
- 348 8. Shea, J. J. Transitions or turnovers? Climatically-forced extinctions of *Homo sapiens*  
349 and Neanderthals in the east Mediterranean Levant. *Quatern. Sci. Rev.* **27**, 2253-2270  
350 (2008).

- 351 9. Mallick, S. *et al.* The Simons Genome Diversity Project: 300 genomes from 142  
352 diverse populations. *Nature* **538**, 201-206 (2016).
- 353 10. Pagani, L. *et al.* Genomic analyses inform on migration events during the peopling of  
354 Eurasia. *Nature* **538**, 238-242 (2016).
- 355 11. Groucutt, H. S. *et al.* Stone tool assemblages and models for the dispersal of *Homo*  
356 *sapiens* out of Africa. *Quatern. Int.* **382**, 8-30 (2015).
- 357 12. Demeter, F., *et al.* Early Modern Humans from Tam Pà Ling, Laos. Fossil Review  
358 and Perspectives. *Curr. Anthropol.* **57**, S17, DOI: 10.1086/694192 (2017)
- 359 13. Westaway, K.E., *et al.* An early modern human presence in Sumatra 73,000-63,000  
360 years ago. *Nature* **548**, 322-325 (2017).
- 361 14. Michel, V., *et al.* The earliest modern *Homo sapiens* in China? *J. Hum. Evol.* **101**,  
362 101-104 (2016).
- 363 15. Liu, W., *et al.* The early unequivocally modern humans in southern China? *Nature*  
364 **526**, 696-699 (2015).
- 365 16. Bae, C., *et al.* Modern human teeth from Late Pleistocene Luna Cave (Guangxi,  
366 China). *Quatern. Int.* **354**, 169-183 (2015).
- 367 17. Liu, W., *et al.* Human remains from Zhiredong, South China, and modern human  
368 emergence in East Asia. *Proc. Natl. Acad. Sci. USA* **107**, 19201-19206 (2010).
- 369 18. Clarkson, C., *et al.* Human occupation of northern Australia by 65,000 years ago.  
370 *Nature* **547**, 306-310 (2017).
- 371 19. Martínón-Torres, M., Wu, X., de Castro, J.M.B., Xing, S., Liu, W. *Homo sapiens* in  
372 the Eastern Asian Late Pleistocene. *Curr. Anthropol.* **58**, S17, DOI: 10.1086/694449.
- 373 20. Groucutt, H. S. & Petraglia, M. D. The prehistory of Arabia: Deserts, dispersals and  
374 demography. *Evol. Anthropol.* **21**, 113-125 (2012).

- 375 21. Petraglia, M. D., Groucutt, H. S., Parton, A. & Alsharekh, A., Green Arabia: Human  
376 prehistory at the Cross-Roads of continents. *Quatern. Int.* **382**, 1-7 (2015).
- 377 22. Jennings, R. P. The greening of Arabia: Multiple opportunities for human occupation  
378 in the Arabian Peninsula during the Late Pleistocene inferred from an ensemble of  
379 climate model simulations. *Quatern. Int.* **205**, 181-199 (2015).
- 380 23. Rosenberg, T. M. *et al.* Middle and Late Pleistocene humid periods recorded in  
381 palaeolake deposits in the Nafud desert, Saudi Arabia. *Quatern. Sci. Rev.* **70**, 109-123  
382 (2013).
- 383 24. Breeze, P. S. *et al.* Palaeohydrological corridors for hominin dispersals in the Middle  
384 East ~250-70,000 years ago. *Quatern. Sci. Rev.* **11**, 155-185 (2016).
- 385 25. Scerri, E. M. L., Drake, N. A., Jennings, R., Groucutt, H.S. Earliest evidence for the  
386 structure of *Homo sapiens* populations in Africa. *Quatern. Sci. Rev.* **101**, 207-216  
387 (2014).
- 388 26. Trinkaus, E. *The Shanidar Neandertals*. (Academic Press, New York, 1981).
- 389 27. McCown T. D. & Keith, A. *The Stone Age of Mount Carmel Volume 2: The fossil*  
390 *human remains from the Levallois-Mousterian* (Clarendon Press, Oxford, 1939).
- 391 28. Vandermeersch, B. *Les hommes fossiles de Qafzeh (Israel)* (CNRS, Paris, 1981).
- 392 29. Walker, M. J., Ortega, J., López, M. V., Parmová, K. & Trinkaus, E. Neanderthal  
393 postcranial remains from the Sima de las Palomas del Cabezo Gordo, Murcia,  
394 Southeastern Spain. *Am. J. Phys. Anthropol.* **144**, 505-515 (2011).
- 395 30. Benjamin, M. *et al.* Where tendons and ligaments meet bone: attachment sites  
396 ('entheses') in relation to exercise and/or mechanical load. *J. Anat.* **208**, 471-490.
- 397 31. Bronk Ramsey, C. Bayesian analysis of radiocarbon dates. *Radiocarbon* **51**, 337-360  
398 (2009).



- 399 32. Drake, N. A., Breeze, P., Parker, A., 2013. Palaeoclimate in the Saharan and Arabian  
400 Deserts during the Middle Palaeolithic and the potential for hominin dispersals.  
401 *Quatern. Int.* **300**, 48-61 (2013).
- 402 33. Parton, A., et al. Orbital-scale climate variability in Arabia as a potential motor for  
403 human dispersals. *Quatern. Int.* **382**, 82-97 (2015).
- 404 34. Vaks, A., Bar-Matthews, M., Matthews, A., Ayalon, A., Frumkin, A. Middle-Late  
405 Quaternary paleoclimate of northern margins of the Saharan-Arabian Desert:  
406 reconstruction from speleothems of Negev Desert, Israel. *Quatern. Sci. Rev.* **29**, 2647-  
407 2662 (2010).
- 408 35. Grant, K.M., et al. The timing of Mediterranean sapropel deposition relative to  
409 insolation, sea-level and African monsoon changes. *Quatern. Sci. Rev.* **140**, 125-141  
410 (2016).
- 411 36. Bar-Matthews, M., Ayalon, A., Gilmour, M., Matthews, A. & Hawkesworth, C. J.  
412 Sea-land oxygen isotopic relationships from planktonic foraminifera and speleothems  
413 in the Eastern Mediterranean region and their implication for paleorainfall during  
414 interglacial intervals. *Geochim. Cosmochim. Acta* **67**, 3181–3199 (2003).
- 415 37. Lisiecki, L. E. & Raymo, M. E. A Pliocene-Pleistocene stack of 57 globally  
416 distributed benthic  $\delta^{18}\text{O}$  records. *Paleoceanography* **20**, 1-17 (2005).
- 417 38. Berger, A. & Loutre, M. F. Insolation values for the climate of the last 10 million  
418 years. *Quatern. Sci. Rev.* **10**, 297-317 (1991).
- 419 39. Fleitmann, D., Burns, S.J., Neff, U., Mangini, A., Matter, A. Changing moisture  
420 sources over the last 333,000 years in Northern Oman from fluid-inclusion evidence  
421 in speleothems. *Quatern. Res.* **60**, 223-232 (2003).
- 422 40. Rosenberg, T.M., et al. Humid periods in southern Arabia: Windows of opportunity  
423 for modern human dispersal. *Geology* **39**, 1115-1118 (2011).

- 424 41. Clark-Balzan, L., Parton., A., Breeze, P.S., Groucutt, H.S., Petraglia, M.D. Resolving  
425 problematic luminescence chronologies for carbonate- and evaporite-rich sediments  
426 spanning multiple humid periods in the Jubbah Basin, Saudi Arabia. *Quatern.*  
427 *Geochron.* <https://doi.org/10.1016/j.quageo.2017.06.002> (2018).
- 428 42. Alonso-Zarza, A. M. Palaeoenvironmental significant of palustrine carbonates and  
429 calcretes in the geological record. *Earth Sci. Rev.* **60**, 261-298 (2003).
- 430 43. Estes, R. D. *The Behaviour Guide to African Mammals* (University of California  
431 Press, Berkeley, 1991).
- 432 44. O'Regan, H. J., Turner, A., Bishop, L. C., Elton, S., Lamb, A. L. Hominins without  
433 fellow travellers? First appearances and inferred dispersals of Afro-Eurasian large-  
434 mammals in the Plio-Pleistocene. *Quatern. Sci. Rev.* **30**, 1343-1352 (2011).
- 435 45. Groucutt, H.S. et al. Human occupation of the Arabian Empty Quarter during MIS 5:  
436 evidence from Mundafan al-Buhayrah. *Quatern. Sci. Rev.* **119**, 116-135 (2015).
- 437 46. Millard, A. R. A critique of the chronometric evidence for hominid fossils: I. Africa  
438 and the Near East 500-50 ka. *J. Hum. Evol.* **54**, 848-874 (2008).
- 439 47. Hublin, J.J., et al. New fossils from Jebel Irhoud, Morocco and the pan-African origin  
440 of *Homo sapiens*. *Nature* **546**, 289-292 (2017).
- 441 48. Richter, D., et al. The age of the hominin fossils from Jebel Irhoud, Morocco, and the  
442 origins of the Middle Stone Age. *Nature* **546**, 293-296 (2017).

443

444

445

446

447

448

449 **Supplementary Information** is available in the online version of the paper.

450

451 **Acknowledgements.** We thank HRH Prince Sultan bin Salman bin Abdulaziz Al-Saud,  
452 President of the Saudi Commission for Tourism and National Heritage (SCTH), and Prof. Ali  
453 Ghabban, Vice President of the SCTH for permission to carry out this study. Dr Zohair  
454 Nawab, President of the Saudi Geological Survey, provided research support and logistics.  
455 Fieldwork and analyses were funded by the European Research Council (no. 295719, to MDP  
456 and 617627, to JTS), the SCTH, the British Academy (HSG and EMLS), The Leverhulme  
457 Trust, the Australian Research Council (DP110101415 to RG, FT150100215 and  
458 TF15010025 to MD, and FT160100450 to JL), and the Research Council of Norway (SFF  
459 Centre for Early Sapiens Behaviour, 262618). We thank Patrick Cuthbertson, Klint Janulis,  
460 Marco Bernal, Salih Al-Soubhi, Mohamad Haptari, Adel Matari, and Yahya Al-Mufarreh for  
461 assistance in the field. We thank Ian Cartwright (Institute of Archaeology, University of  
462 Oxford) for the photographs of AW-1 (Fig. 2a), Ian Matthews (RHUL) for producing the  
463 Bayesian age model, and Michelle O'Reilly (MPI-SHH) for assistance with the preparation  
464 of figures. We acknowledge the Max Planck Society for supporting us with comparative  
465 fossil data, and we thank curators for access to comparative extant and fossil material in their  
466 care (Supplementary Tables 5 and 7).

467

468 **Author Contributions** H.S.G. and M.D.P. designed, coordinated and supervised the study.  
469 H.S.G., I.S.Z., N.D, S.A., I.C., R.C-W., J.L., P.S.B., M.S., G.J.P., A.A., A.A.-O., A.M. B.A.,  
470 E.M.L.S. and M.D.P. conducted excavation, survey and multidisciplinary sampling at Al  
471 Wusta. L.T.B., T.L.K., E.P., N.B.S and J.T.S. conducted the morphological analysis and  
472 comparative study of the AW-1 phalanx. R.G., M.D. and L.K. carried out the U-series and  
473 ESR analyses. S.J.A. and R.C.W carried out the OSL dating. I.C. and R.C.W conducted the

474 stratigraphic and sedimentological analysis of the site, with input from N.D., J.L. and G.J.P.  
475 W.W.S. analysed the diatoms. M.S. and J.L. analysed the vertebrate fossils, with input from  
476 G.J.P. Lithic analysis was conducted by H.S.G. and E.M.L.S. Spatial analyses were  
477 conducted by P.S.B. All authors helped to write the paper.

478

479 **Author Information** The authors declare no competing financial interests.

480 Readers are welcome to comment on the online version of the paper.

481 Correspondence and requests for materials should be addressed to

482 H.S.G. (huw.groucutt@rlaha.ox.ac.uk) or M.D.P. (petraglia@shh.mpg.de).

483

484 **Data availability statement.** Authors can confirm that all relevant data are included in the  
485 paper and/ or its supplementary information files.

486

487

488

489

490

491

492

493

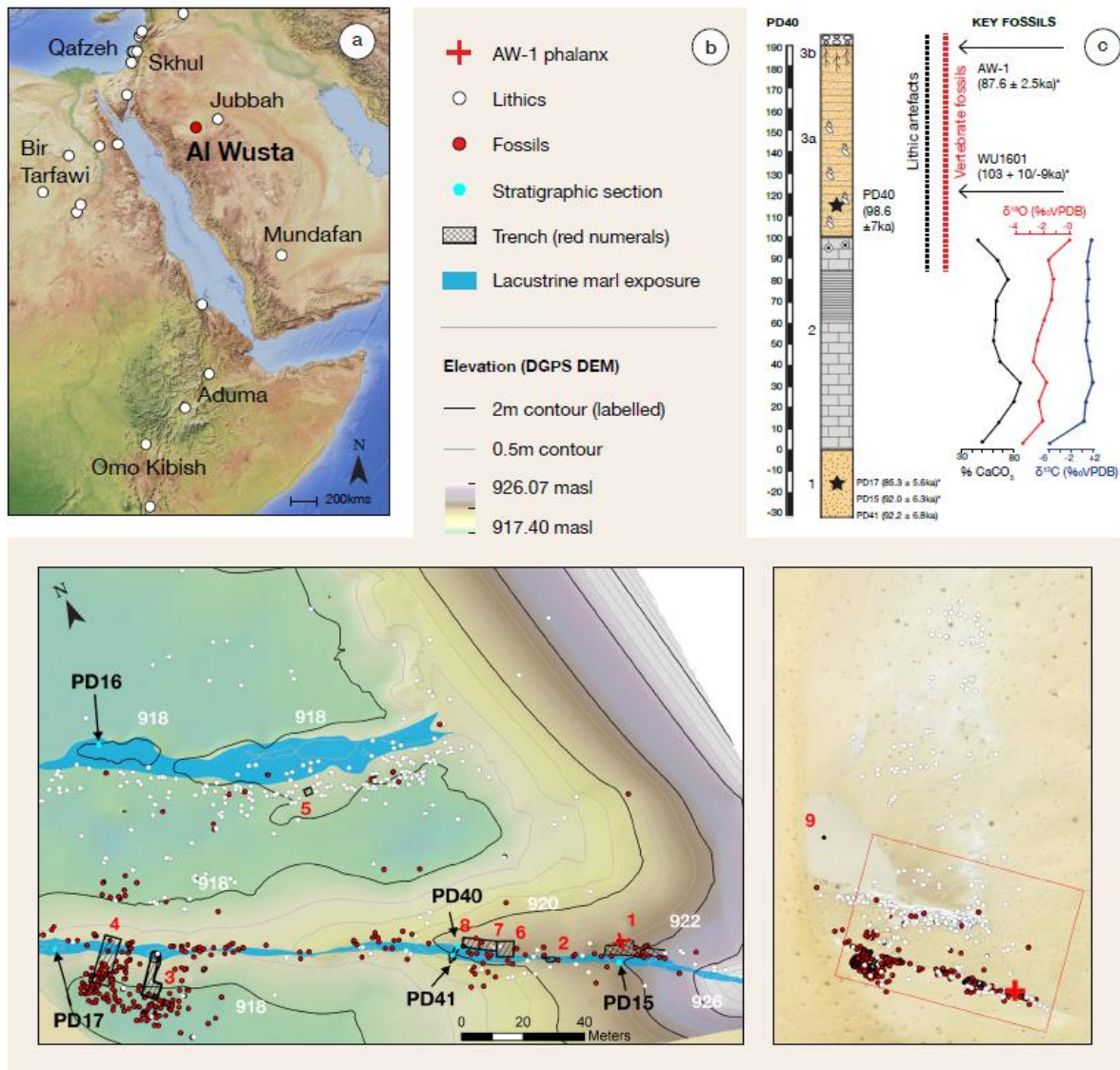
494

495

496

497

498

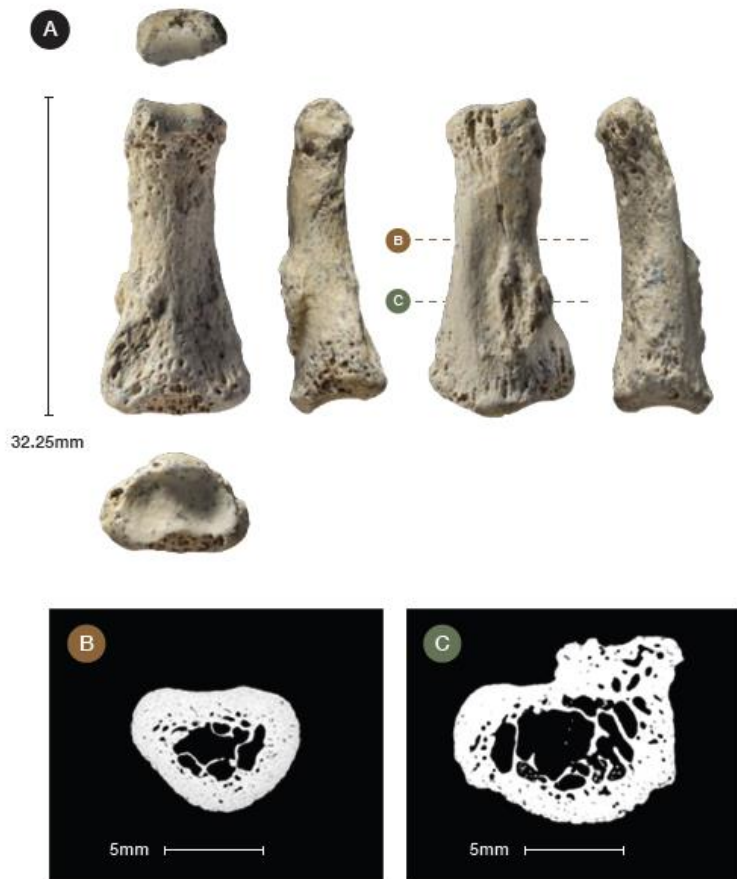


501

502 **Figure 1. Al Wusta location, map of site and stratigraphy.** A: The location of Al Wusta  
 503 and other key MIS 5 sites in the region<sup>11</sup>; B: Al Wusta digital elevation model showing  
 504 location of AW-1 phalanx, marl beds, lithics and vertebrate fossils, and the locations of the  
 505 trenches and sections. The inset shows a satellite image of the site; C: Stratigraphic log of Al  
 506 Wusta showing the sedimentology of the exposed carbonate beds, isotopic values, OSL ages  
 507 for sand beds and U-series and ESR ages for AW-1 and WU-1601. Sands are shown in  
 508 yellow: lower massive sands are aeolian (Unit 1), upper laminated sands are waterlain (Unit

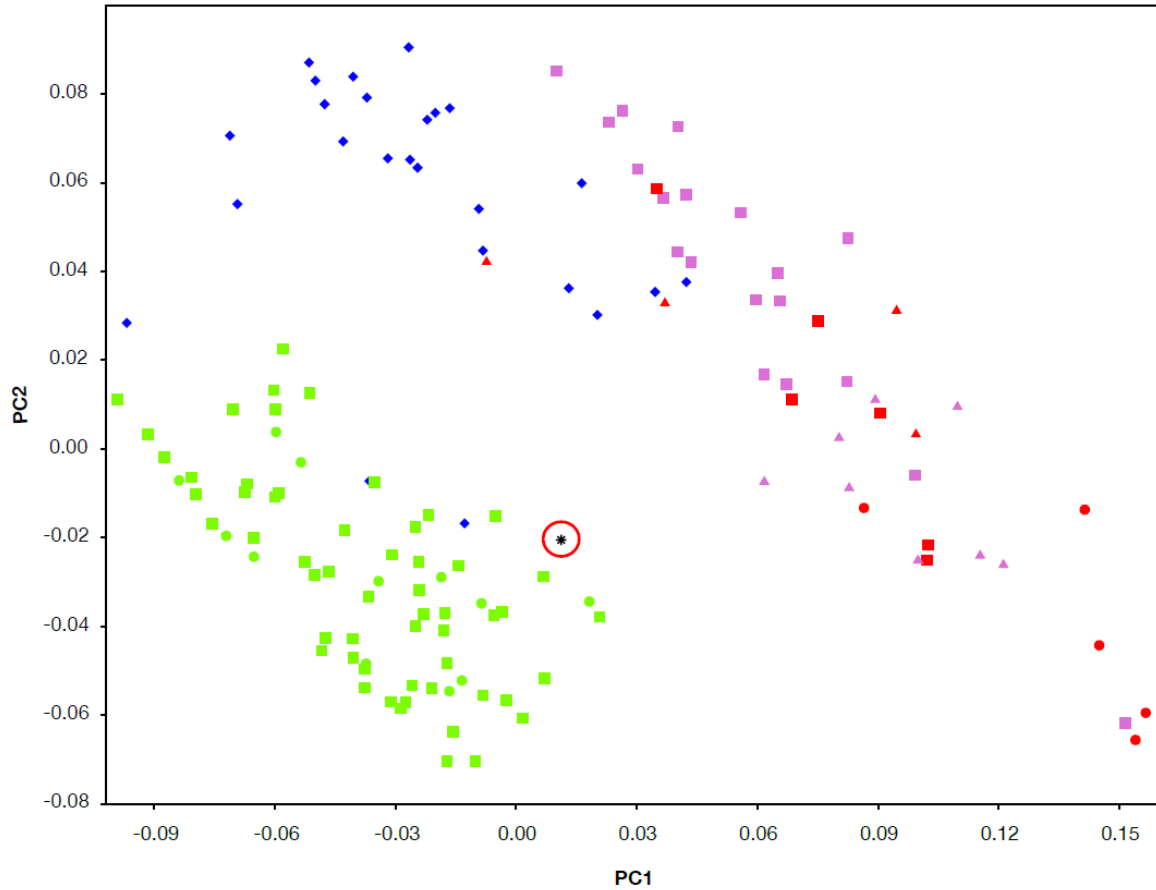
509 3a) and have been locally winnowed to generate a coarse desert pavement (Unit 3b),  
510 lacustrine marls are shown (Unit 2) in grey (for full key and description see Supplementary  
511 Figures 13 and 14 and Supplementary Information 5). Section PD40 is shown as it contains  
512 the thickest sequence and is most representative of Al Wusta, chronometric age estimates  
513 (marked \*) from the site are depicted in their relative stratigraphic position, see  
514 Supplementary Figure 14 for their absolute positions.

515



516

517 **Figure 2. Photographs and micro-CT scans of Al Wusta-1 *Homo sapiens* phalanx. A:**  
 518 photographs in (left column, top to bottom) distal, palmar and proximal views, and (middle  
 519 row, left to right) lateral 1, dorsal and lateral 2 views. Micro-CT cross-sections (illustrated at  
 520 2x magnification) include B (54% from proximal end) and C (illustrating abnormal bone).



521

522 **Figure 3. Scatterplot of the first two principal components (PC) scores of the geometric**

523 **morphometric analysis of the Al Wusta-1 phalanx compared with a sample of primates,**

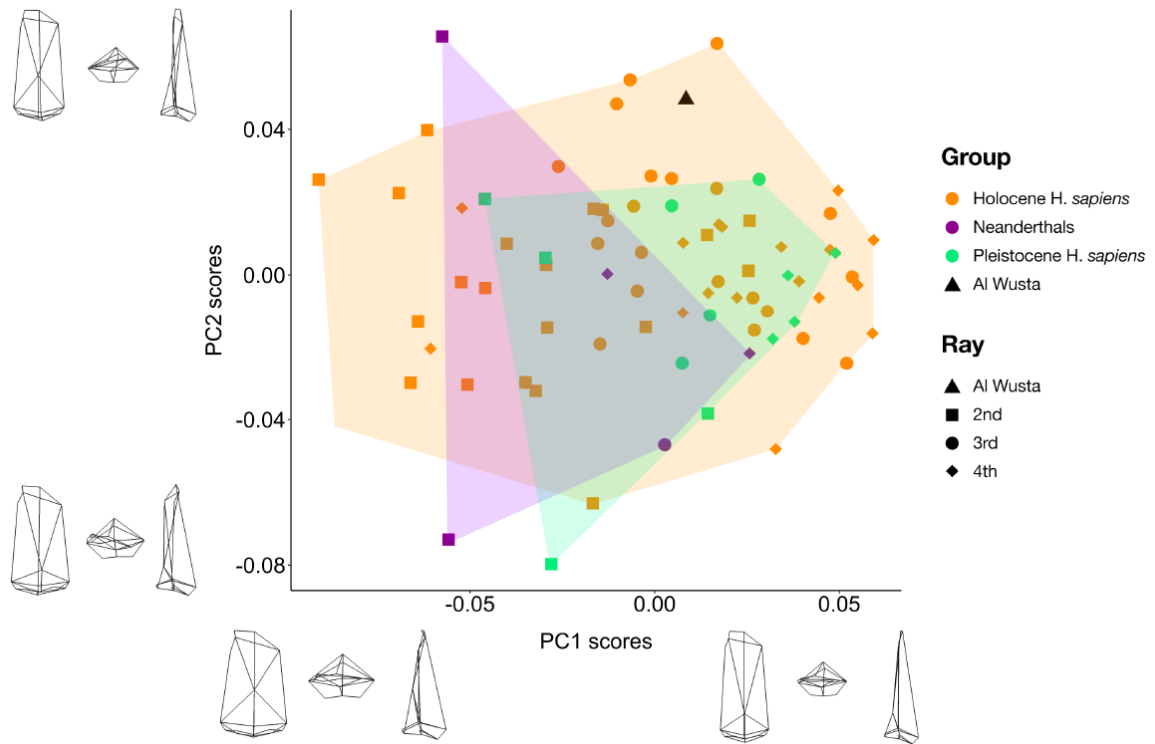
524 **including hominins.** Non-human hominoids: lilac; *Gorilla*: circles, *Pan*: triangles.

525 Cercopithecoids: red; *Colobus*: triangles, *Mandrillus*: squares, *Papio*: circles. Neanderthals:

526 blue diamonds. *H. sapiens*: green; early *H. sapiens*: circles, Holocene *H. sapiens*: squares. Al

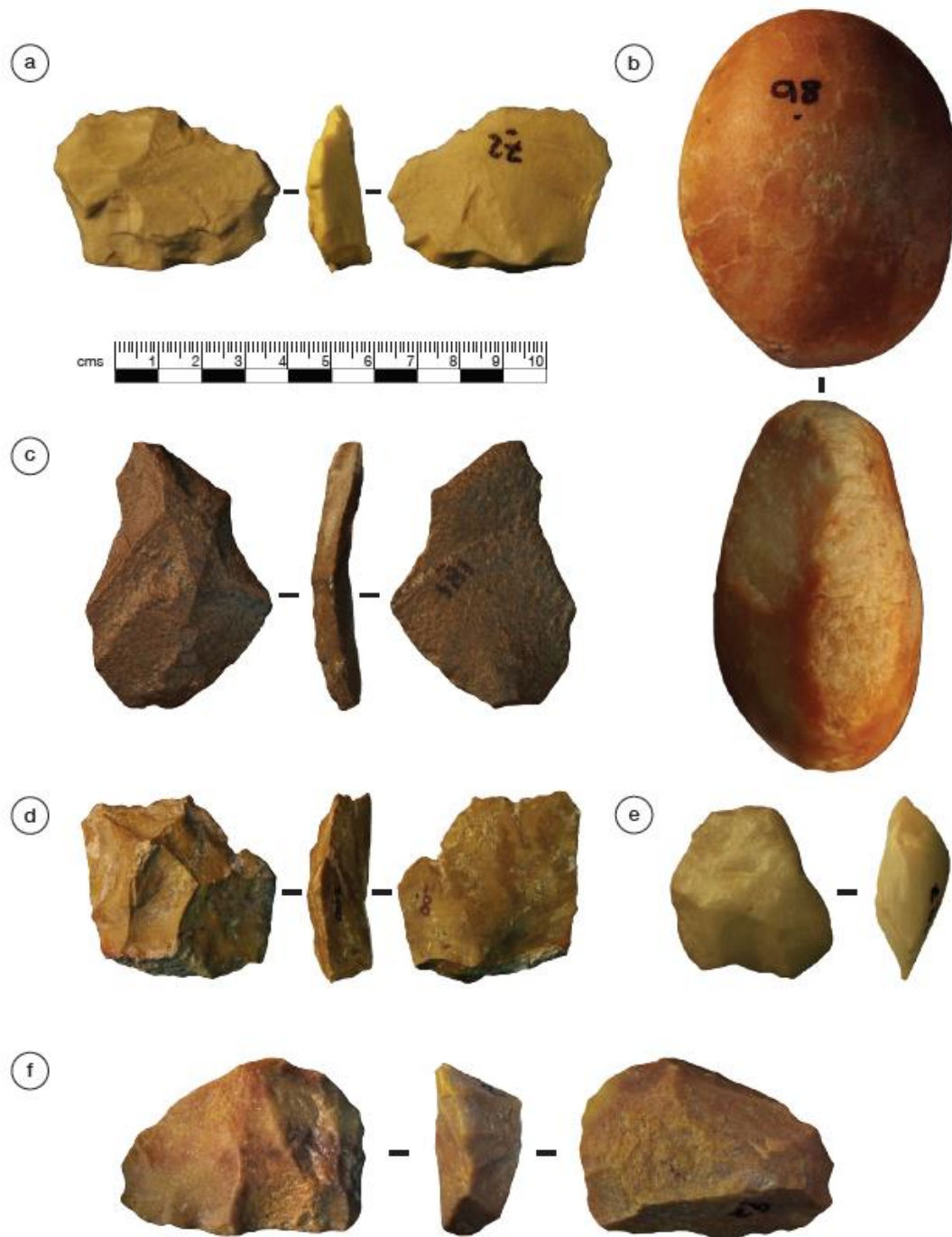
527 Wusta-1: black star, circled in red.





528

529 **Figure 4: Scatterplot of the first two principal component (PC) scores from the**  
 530 **geometric morphometric analyses of AW-1 and sample of comparative hominin 2<sup>nd</sup>, 3<sup>rd</sup>,**  
 531 **and 4<sup>th</sup> intermediate phalanges.** Wireframes show mean configuration warped to extremes  
 532 of PC axes in dorsal (left), proximal (middle) and lateral (right) views. Convex hulls added  
 533 post-hoc to aid visualisation.



534

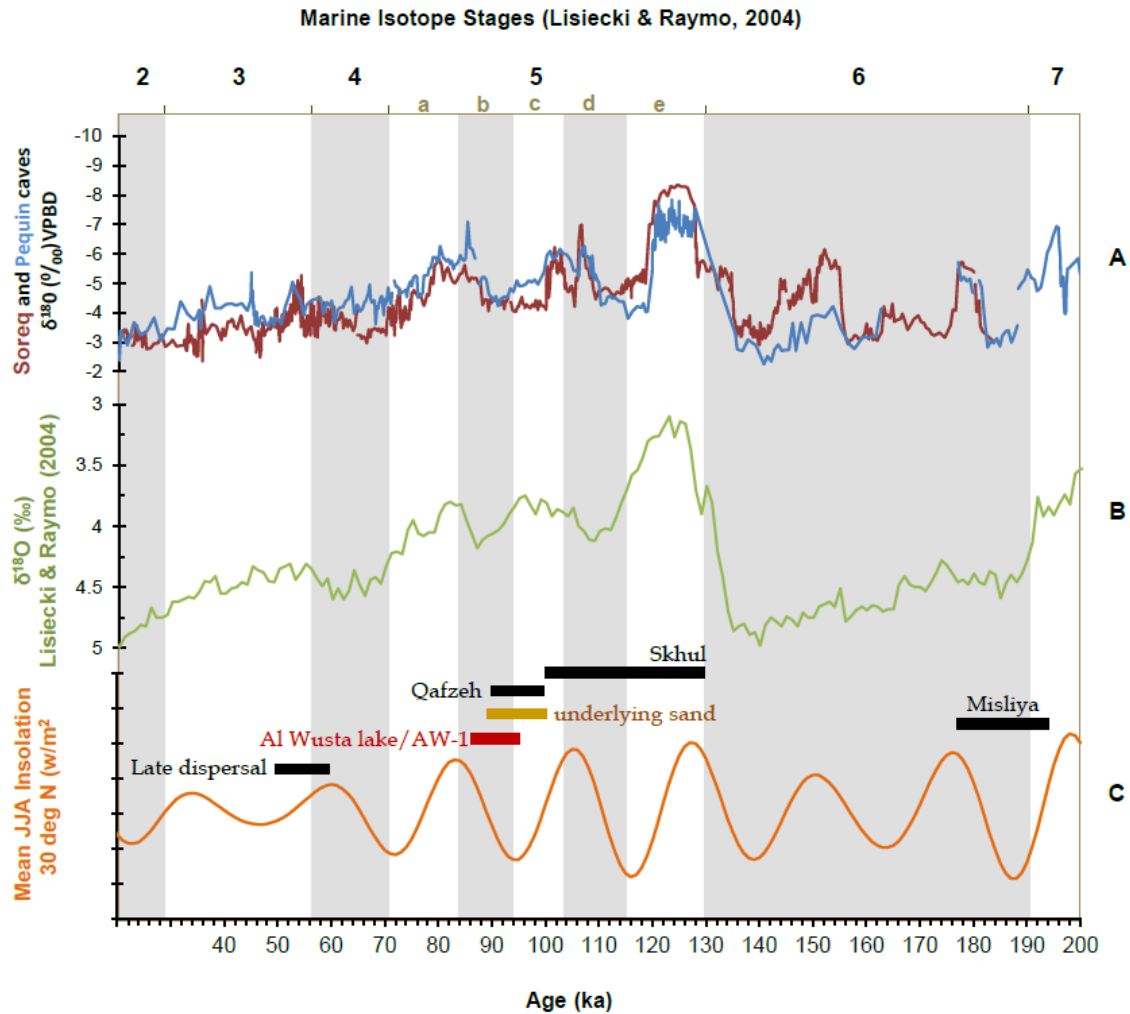
535 **Figure 5. Selected Al Wusta lithic artefacts.** A: argillaceous quartzite flake; B: quartz

536 hammerstone; C: ferruginous quartzite Levallois flake; D: chert Levallois flake; E: Quartz

537 recurrent centripetal Levallois core; F: quartzite preferential Levallois core with centripetal

538 preparation and pointed preferential removal.

539



540  
 541 **Figure 6. The chronological and climatic context of Al Wusta.** The Al Wusta lake phase  
 542 falls chronologically at the end of the time-range of MIS 5 sites from the Mediterranean  
 543 woodland of the Levant (~130-90 ka) and earlier than the late dispersal(s) (~60-50 ka) as  
 544 posited in particular by genetic studies. The chronology of these dispersals and occupations  
 545 correspond with periods of orbitally modulated humid phases in the eastern Mediterranean<sup>36</sup>  
 546 that are important intervals for human dispersals into Eurasia, and are also proposed to  
 547 correspond with episodes of monsoon driven humidity in the Negev and Arabian desert<sup>34</sup>.  
 548 Environmental amelioration of the Saharo-Arabian belt, therefore, appears to be crucial for  
 549 allowing occupation at key sites that document dispersal out of Africa. A: East Mediterranean  
 550 speleothem  $\delta^{18}\text{O}$  record from Soreq and Pequin Caves<sup>36</sup>; B: global  $\delta^{18}\text{O}$  record<sup>37</sup>; C:

551 Insolation at 30 degrees north<sup>38</sup>, showing the temporal position of key sites relating to  
552 dispersal out of Africa<sup>2,3,11,48</sup>. The chronology for Al Wusta shows the phases defined by the  
553 Bayesian model at  $2\sigma$ .

554

555

556

557

558

559

560

561

562

563

564

565

566

567

568

569

570

571

572

573

574

575

576 **Methods**

577

578 **Site identification, survey and excavation.** The site of Al Wusta (field code WNEF16\_30)  
579 was discovered in 2014 as part of a programme of joint survey fieldwork of the Palaeodeserts  
580 Project, the Saudi Commission for Tourism and National Heritage, and the Saudi Geological  
581 Survey. It is located in the western Nefud desert, a few kilometres from the Middle  
582 Pleistocene fossil locality of Ti's al Ghaddah<sup>49</sup>. The locations of all materials of interest  
583 (fossils, stone tools, geomorphological features, excavations and sample points) were  
584 recorded using a high-precision Trimble XRS Pro Differential GPS system and a total station,  
585 and entered into a GIS (Fig. 1). Elevation data (masl) were recorded as a series of transects  
586 across the site, and a digital elevation model (DEM) and contours interpolated (Spline) from  
587 all data with precisions of better than 10 cm in all (x,y,z) dimensions (22,047 points). This  
588 allowed visualisation and recording of the spatial relationships between materials in three  
589 dimensions (Fig. 1). Eight trenches were excavated into the fossil and artefact bearing  
590 deposits. These trenches revealed vertebrate remains and lithics, but no further human fossils  
591 were recovered.

592

593 **Morphological analysis of Al Wusta-1 phalanx.** The phalanx was scanned using micro-  
594 computed tomography (micro-CT) on the Nikon Metrology XT H 225 ST High Resolution  
595 scanner and X-Tek software (Nikon Metrology, Tring, UK) housed in the Cambridge  
596 Biotomography Centre, University of Cambridge, UK. Scan parameters were: a tungsten  
597 target; 0.5 mm copper filter; 150 kV; 210 mA; 1080 projections with 1000 ms exposure, and  
598 resulted in a voxel size of 0.02 mm<sup>3</sup>. The micro-CT data were reconstructed using CT-PRO  
599 3D software (Nikon Metrology) and exported as an image (.tif) stack. Other CT data were

600 obtained from the institutions cited in Supplementary Table 5 with permissions following the  
601 memoranda of understanding with each institution.

602

603 3D landmarks and semilandmarks were chosen to best describe the overall shape of the  
604 morphology of the AW-1 phalanx (Supplementary Table 4, Supplementary Figure 2), and  
605 were digitised on virtual reconstructions of phalanges created from micro-CT data in AVIZO  
606 8 and 9.1 (FEI Software, Burlington, Mass.). Landmark coordinates were exported for use in  
607 Morphologika<sup>50</sup>. In Morphologika, generalized Procrustes analyses were performed to  
608 superimpose landmark coordinate data, and principal components analyses (PCA) were run  
609 to investigate similarities in shape between specimens. Shape differences along principal  
610 componentss were visualised and wireframes were produced in Morphologika, PC scores  
611 were exported to create graphs in R<sup>51</sup>. Procrustes distances between specimens were  
612 calculated using MorphoJ<sup>52</sup>. To avoid representing the same phalanges from different sides of  
613 a single individual as independent data points and to maximise sample sizes in pooled  
614 analyses, right phalanges were used in cases where the phalanges from both sides were  
615 present. Where only the left was present, this was used and ‘reflected’ (i.e. mirrored) in  
616 Morphologika to generate landmark configurations consistent with right phalanges.

617

618 **U-series and combined US-ESR dating of fossil bone and teeth.** The AW-1 phalanx (lab  
619 number 3675) and a hippopotamus tooth fragment (lab number WU1601) were collected  
620 from Trench 1 (Fig.1) for U-series and combined US-ESR dating, respectively. The external  
621 dose rate utilised the data of OSL sample PD40, which was collected in an equivalent  
622 position within unit 3a.

623

624 *U-series analysis.* U-series analyses were conducted at the Research School of Earth  
625 Sciences, The Australian National University, Canberra. The experimental setup for the U-  
626 series analysis of the phalanx was described in detail by Grün and colleagues<sup>53</sup>  
627 (Supplementary Figures 2 and 3, Supplementary Information 2). Laser ablation (LA) was  
628 used to drill a number of holes into AW-1 following the approach of Benson and  
629 colleagues<sup>54</sup>. After a cleaning run with the laser set at a diameter of 460  $\mu\text{m}$ , seven holes were  
630 drilled for 1000 s with the laser set at 330  $\mu\text{m}$ . The isotopic data streams were converted into  
631  $^{230}\text{Th}/^{234}\text{U}$  and  $^{234}\text{U}/^{238}\text{U}$  activity ratios and apparent Th/U age estimates and subsequently  
632 binned into 30 successive sections (each containing 33 cycles) for the calculation of average  
633 isotopic ratios and ages. A similar experimental setup and methodology were employed for  
634 the LA U-series analysis of tooth sample WU1601. The whole closed system U-series  
635 analytical datasets of the enamel and dentine sections were integrated to provide the data  
636 input for the ESR age calculations.

637

638 *Combined US-ESR dating of the fossil tooth: ESR dose evaluation.* The ESR dose evaluation  
639 of the hippo tooth was carried out at CENIEH, Burgos, Spain, following a similar procedure  
640 to that described in Stimpson and colleagues<sup>49</sup>. Enamel was collected from WU1601 and  
641 powdered <200  $\mu\text{m}$ . The sample was then divided into 11 aliquots and gamma irradiated with  
642 a Gammacell-1000 Cs-137 source to increasing doses until 3.4 kGy. ESR measurements were  
643 carried out at room temperature with an EMXmicro 6/1 Bruker ESR spectrometer coupled to  
644 a standard rectangular ER 4102ST cavity. ESR intensities were extracted from T1-B2 peak-  
645 to-peak amplitudes of the ESR signal of enamel. Fitting procedures were carried out with a  
646 single saturating exponential (SSE) function through the pooled ESR experimental data  
647 derived from the repeated measurements, with data weighting by the inverse of the squared  
648 ESR intensity ( $1/I^2$ ) and following the recommendations by Duval and Grün<sup>55</sup>. Full details

649 about the experimental conditions and analytical procedure may be found in Supplementary  
650 Information 2.

651

652 *Combined US-ESR dating of the fossil tooth: Dose rate evaluation and age calculations.* The  
653 combined US-ESR age of WU1601 was calculated with the DATA programme<sup>56</sup> using the  
654 US model defined by Grün and colleagues<sup>57</sup>. The following parameters were used for the  
655 dose rate evaluation: an alpha efficiency of  $0.13 \pm 0.02$ <sup>58</sup>, Monte-Carlo beta attenuation  
656 factors from Marsh<sup>59</sup>, dose-rate conversion factors from Guerin and colleagues<sup>60</sup>, external  
657 sediment (beta and gamma) dose rate from the OSL sample PD40, a depth of  $25 \pm 10$  cm,  
658 resulting in an age of  $103 + 10/-9$  ka.

659

660 **Optically Stimulated Luminescence Dating.** Three samples (PD15, PD17 and PD41) were  
661 collected from the aeolian sands (Unit 1) underlying the southern marl outcrop (Unit 2, Fig  
662 1B). A fourth sample (PD40) was taken from the main fossil bearing bed (Unit 3). Individual  
663 quartz grains were measured on a Risø TL/OSL-DA-15 instrument using the single-aliquot  
664 regenerative-dose (SAR) method<sup>61</sup>. The burial dose for each sample ( $D_b$ ) was calculated  
665 using the central age model (CAM)<sup>62</sup>.

666

667 Environmental dose rates were determined using a Risø GM-25-5 low-level beta counting  
668 system<sup>63</sup> (beta dose rate), field gamma spectrometry (gamma dose rate), and an estimate of  
669 the cosmic dose rate derived using site location and present day sediment burial depths<sup>64</sup>. Full  
670 optically stimulated luminescence dating methods and results are presented in Supplementary  
671 Information Section 3. All analyses were carried out in the Royal Holloway Luminescence  
672 Laboratory by SA and R C-W.

673



674 **Age modelling.** Chronometric ages for samples from the Al Wusta site were incorporated  
675 into a Bayesian sequential phase model implemented in OxCal v4.2<sup>31</sup> (Supplementary  
676 Information 4; Supplementary Figure 11. The model consists of two discrete phases separated  
677 by a hiatus. Phase 1 was defined by the three OSL ages (PD15, 17 and 41) for samples from  
678 the aeolian sands (Unit 1) underlying the lacustrine marls (Unit 2). Phase 2 was defined by  
679 the ages for the sand (PD40) and fossils (AW-1 and WU1601) from the waterlain sediments  
680 (Unit 3) overlying Unit 2. U-series ages for WU1601 and AW-1 were treated as minimum  
681 age estimates, whereas PD40 and the combined U-series-ESR age on WU1601 were treated  
682 as finite age estimates. Since the Al Wusta sequence accumulated over a short period of time,  
683 and contains only five finite ages (and three minimum ages), the General Outlier Model<sup>31</sup> was  
684 unable to function, and instead a simpler model using agreement indices was employed. This  
685 analysis yielded Amodel (76) and Aoverall (79) values well in excess of the generally  
686 accepted threshold (60<sup>31</sup>), with only one age yielding an individual agreement index below  
687 this threshold (PD17, 51). These data indicate that no ages should be excluded from the  
688 model, and that the age model itself is robust. The Bayesian sequential model yielded an age  
689 for the end of Phase 1 of  $93.1 \pm 2.6$  ka (1  $\sigma$  uncertainties), while Phase 2 yielded start and end  
690 dates of  $92.2 \pm 2.6$  ka and  $90.4 \pm 3.9$  ka respectively. The end date for phase 2 should be  
691 treated as a maximum value since no overlying material is present, precluding the possibility  
692 of further constraining the end of this phase.

693

#### 694 **Stratigraphy and sedimentology.**

695 *Sediment analysis.* Bulk samples (in the form of coherent blocks) were taken at 10 cm  
696 intervals through each of the marl beds in four sections (Fig. 1C and Supplementary Figures  
697 13 and 14). Each block was air-dried and subsamples (ca 0.5 g) were removed, powdered and  
698 analysed for percentage carbonate content using Bascomb calcimetry, which measures the

699 volume of carbon dioxide liberated from a known sample mass during reaction with 10%  
700 HCl<sup>65</sup>. Thin sections were prepared from fresh sediment blocks. The sediments did not  
701 require acetone treatment as they were already dry and, due to their permeability, were  
702 impregnated with a bonding resin. Standard thin section preparation was then carried out  
703 using techniques developed in the Centre for Micromorphology at Royal Holloway,  
704 University of London<sup>66</sup>. Thin sections were analysed using an Olympus BX-50 microscope  
705 with magnifications from 20x to 200x and photomicrographs were captured with a Pixera  
706 Penguin 600es camera. A point-count approach was used to produce semi-quantified data  
707 from the thin sections, based on counting micro-features at 3 mm intervals along linear  
708 transects 1 cm apart. Kemp<sup>67</sup>, Stoops<sup>68</sup> and Alonso-Zarza<sup>42</sup> were referred to when identifying  
709 features. X-ray diffraction analysis (XRD) was carried out in the Department of Earth  
710 Sciences (Royal Holloway, University of London). Powdered samples were analysed on a  
711 Philips PW1830/3020 spectrometer with copper K $\alpha$  X-rays. Mineral peaks were identified  
712 manually from the ICDD Powder Diffraction File (PDF) database. The methods and results  
713 are described further in Supplementary Information 5.

714

715 *Diatoms.*

716 *Sample preparation.* Samples were analysed using the standard method of Renberg<sup>69</sup>  
717 (Supplementary Information 5). Thus, all samples were treated with 30% H<sub>2</sub>O<sub>2</sub> and 5% HCl  
718 to digest organic material and remove calcium carbonate. Distilled water was added to dilute  
719 the samples after heating, which were then stored in the refrigerator for four days to minimise  
720 further chemical reactions. The samples were rinsed daily and allowed to settle overnight. A  
721 known volume of microspheres was added to the supernatant after the last rinse to enable  
722 calculation of the diatom concentration<sup>70</sup>. The slides were air-dried at room temperature in a  
723 dust free environment before mounting with Naphrax diatom mountant. Diatom taxonomy

724 followed Krammer and Lange-Bertalot<sup>71-73</sup> and taxonomic revisions<sup>74,75</sup> with at least 300  
725 valves enumerated for a representative sample at x1000 magnification.  
726  
727 *Numerical analysis.* Prevalent trends in the diatom assemblage were explored using  
728 ordination analyses using CANOCO 4.5 of ter Braak and Šmilauer<sup>76</sup>. Detrended  
729 Correspondence Analysis (DCA<sup>77</sup>) with detrending by segments and down-weighting of rare  
730 species was used to investigate taxonomic variations within each site and to determine  
731 whether linear or unimodal models should be used for further analyses. If the gradient length  
732 of the first axis is <1.5 SD units, linear methods (Principle Component Analysis, PCA)  
733 should be used; however, if the gradient length is >1.5 SD units, unimodal methods  
734 (Correspondence Analysis) should be used<sup>78</sup>. Detrended Canonical Correspondence Analysis  
735 (DCCA<sup>79</sup>) was also used to show changes in compositional turnover scaled in SD units.  
736 Therefore, variations in the down-core DCCA first axis sample scores show an estimate of  
737 the compositional change between samples along an environmental or temporal gradient.  
738 Depth was used as the sole constraint as the samples in each site are in a known temporal  
739 order<sup>80</sup>. The dataset was square-root transformed to normalise the distribution prior to  
740 analyses. Optimal sum-of-squares partitioning<sup>81</sup> with the program ZONE<sup>82</sup> and comparison of  
741 the zones with the Broken-stick model using the program BSTICK<sup>83</sup> were used to determine  
742 significant zones. The planktonic: benthic ratio, habitat summary, concentration and the F  
743 index (a dissolution index<sup>84</sup>) were calculated for all the samples.

744

#### 745 *Stable isotopes*

746 It is common practice, when analysing the  $\delta^{18}\text{O}$  and  $\delta^{13}\text{C}$  values of lacustrine/palustrine  
747 carbonates to either: 1) sieve the sediment and analyse the <63 $\mu\text{m}$  fraction, or 2) use the  
748 microstructure of the sample, as identified under thin section, to identify pure, unaltered

749 fabrics, which can then be drilled out and analysed<sup>85</sup>. The former procedure ensures that the  
750 analysed fraction comprises pure authigenic marl (rather than a mixture of ostracod,  
751 mollusc, chara and marl components that will contain different isotopic values). The latter is  
752 done to ensure that any carbonate that has been affected by diagenesis is sampled. Neither of  
753 these approaches were carried out here as; 1) microfabric analysis showed no evidence for  
754 diagenesis (although some of the samples are cemented the cement makes a negligible  
755 component of sample mass), and 2) some of the samples have incipient cementation, which  
756 means that they cannot be sieved. Bulk carbonate powders were consequently analysed for  
757  $\delta^{18}\text{O}$  and  $\delta^{13}\text{C}$ . To show that the analysis of bulk samples had no impact on the derived  
758 isotopic data, samples that were friable enough to be sieved were treated with sodium  
759 hexametaphosphate to disaggregate them and then homogenised and separated into two  
760 subsamples for isotopic analysis; (1) a sieved  $<63\mu\text{m}$  fraction and (2) a homogenised bulk  
761 sample. The resulting isotopic data showed no difference between the  $\delta^{18}\text{O}$  and  $\delta^{13}\text{C}$  values  
762 of the sieved and bulk samples (Supplementary Figure 13b), highlighting that the  
763 homogenous and unaltered nature of the material results in bulk carbonate isotopic analysis  
764 generating valid data. Two samples were taken from different locations of each sampled  
765 block to generate a larger dataset of independent samples. The  $\delta^{18}\text{O}$  and  $\delta^{13}\text{C}$  values of each  
766 samples were determined by analysing  $\text{CO}_2$  liberated from the reaction of the sample with  
767 phosphoric acid at  $90^\circ\text{C}$  using a VG PRISM series 2 mass spectrometer in the Earth Sciences  
768 Department at Royal Holloway. Internal (RHBNC) and external (NBS19, LSVEC) standards  
769 were run every 4 and 18 samples respectively.  $1\sigma$  uncertainties are  $0.04\text{‰}$  ( $\delta^{18}\text{O}$ ) and  $0.02\text{‰}$   
770 ( $\delta^{13}\text{C}$ ). All isotope data presented in this study are quoted against the Vienna Pee Dee  
771 Belemnite (VPDB) standard.

772

773 **Vertebrate fossil analyses.** Each fossil specimen was identified to lowest taxonomic and  
774 anatomical level possible (Supplementary Figure 20, Supplementary Table 19 and  
775 Supplementary Information 6). Taxonomic identification and skeletal element portions were  
776 determined based on anatomical landmarks, and facilitated by comparisons with the  
777 Australian National University Archaeology and Natural History reference collection  
778 (Canberra), unregistered biological collections held at the University of New South Wales  
779 (Sydney), and the large mammal collections of the Zoologische Staatssammlung München  
780 (Munich). Each specimen was assigned a size category (small, medium, and large) following  
781 Dominguez-Rodrigo and colleagues<sup>86</sup>, and corresponding to the five size classes described in  
782 Bunn<sup>87</sup>, where small, medium and large denote size classes 1-2, 3A-3B and 4-6, respectively.  
783 Element abundance is reported as Number of Identified Specimens (NISP).

784

785 Each specimen was examined for modification by eye and hand-lens (10x) under both natural  
786 and high-incidence light, and examined at different angles to assist identification of fine-scale  
787 surface modifications. Where required, further examination and photography was carried out  
788 using a digital microscope (Model: Dino-lite, AM7013MZ). Morphometric data (length,  
789 breadth and width) was measured using digital callipers (Model: Mitutoyo Corp, CD-  
790 8"PMX), and specimen weights using a digital scale. Bone surface modifications were  
791 identified and recorded following standard methodologies: butchery and tooth marks<sup>88-94</sup>,  
792 burning<sup>95-96</sup>, rodent gnawing<sup>97,98</sup>, weathering<sup>99</sup> and trampling<sup>100</sup>. Carnivore damage was  
793 categorized as pit, score, furrow or puncture, and the location noted<sup>94</sup>. Tooth mark  
794 morphometric data – short and long axes – was also recorded. Any additional modifications,  
795 i.e. polish, manganese staining, and root etching, were also reported and described. Bone  
796 breakage was recorded as green, dry, or both, following Villa and Mahieu<sup>101</sup>. Long bone

797 circumference completeness was recorded using the three categories described by Bunn<sup>102</sup>:  
798 type 1 (<1/2), type 2 (>1/2 but < complete) and type 3 (complete).

799

800 **Lithic analysis.** Lithics were systematically collected during pedestrian transects and  
801 excavations of Al Wusta. This produced a total studied assemblage of 380 lithics  
802 (Supplementary Information 7). Further lithics extended for a considerable distance to the  
803 north, seeming to track the outlines of the palaeolake, but we only conducted detailed  
804 analysis on lithics from the southern part of the site, close to AW-1 and the sedimentary ridge  
805 on which it was found (i.e. south of the Holocene playa). These were analysed using the  
806 methodology described in Scerri and colleagues<sup>25,103,104</sup> and Groucutt and colleagues<sup>45,105</sup>. As  
807 well as qualitative analysis of technological features indicating particular techniques and  
808 methods of reduction, a variety of quantitative features such as dimensions, the number of  
809 scars and % of cortex were recorded. Informative examples were selected for photography  
810 and illustration. This approach allows both a characterisation and description of the  
811 assemblage and broad comparison with other assemblages from surrounding regions.

812

813

814

815

816

817

818

819

820

821

822 **Methods References**

823

824 49. Stimpson, C. et al. Middle Pleistocene vertebrate fossils from the Nefud Desert, Saudi  
825 Arabia: Implications for biogeography and palaeoecology. *Quatern. Sci. Rev.* **143**, 13-  
826 36 (2016).

827 50. O'Higgins, P., Jones, N. Facial growth in *Cercocebus torquatus*: an application of  
828 three-dimensional geometric morphometric techniques to the study of morphological  
829 variation. *J. Anat.* **193**, 251-72 (1998).

830 51. R Core Team. *R: A Language and Environment for Statistical Computing*. (Vienna,  
831 Austria: R Foundation for Statistical Computing, <http://www.R-project.org>, 2015).

832 52. Klingenberg C, P. MorphoJ: an integrated software package for geometric  
833 morphometrics. *Mol. Ecol. Resour.* **11**, 353-7 (2011)

834 53. Grün, R., Eggins, S., Kinsley, L., Mosely, H., Sambridge, M. Laser ablation U-series  
835 analysis of fossil bones and teeth. *Palaeogeogr., Palaeoclimatol., Palaeoecol.* **416**,  
836 150-167 (2014).

837 54. Benson, A., Kinsley, L., Defleur, A., Kokkonen, H., Mussi, M., Grün, R. Laser  
838 ablation depth profiling of U-series and Sr isotopes in human fossils. *J. Arch. Sci.* **40**,  
839 2991-3000 (2013).

840 55. Duval, M., Grün, R. Are published ESR dose assessments on fossil tooth enamel  
841 reliable? *Quat. Geochron.* **31**, 19-27 (2016).

842 56. Grün, R. The DATA program for the calculation of ESR age estimates on tooth  
843 enamel. *Quatern. Geochron.* **4**, 231-232 (2009).

844 57. Grün, R., Schwarcz, H.P., Chadam, J. ESR dating of tooth enamel: Coupled  
845 correction for U-uptake and U-series disequilibrium. *Int. J. Radiat. Appl. Instrum.*  
846 *Nucl. Tracks. Radiat. Meas.* **14**, 237-241 (1988).

- 847 58. Grün, R., Katzenberger-Apel, O. An alpha irradiator for ESR dating. *Ancient TL* **12**,  
848 35-38 (1994).
- 849 59. Marsh, R. E. Beta-gradient Isochrons Using Electron Paramagnetic Resonance:  
850 Towards a New Dating Method in Archaeology. (MSc thesis, McMaster University,  
851 Hamilton, 1999).
- 852 60. Guérin, G., N. Mercier and G. Adamiec. Dose-rate conversion factors: update.  
853 *Ancient TL* 29(1): 5-8 (2011).
- 854 61. Murray, A. S., Wintle, A. G. Luminescence dating of quartz using an improved  
855 single-aliquot regenerative-dose protocol. *Radiat. Meas.* **32**, 57-73 (2000).
- 856 62. Galbraith, R. F., Roberts, R. G., Laslett, G. M., Yoshida, H., Olley, J. M. Optical  
857 dating of single and multiple grains of quartz from Jinmium rock shelter, northern  
858 Australia: Part I, experimental design and statistical models. *Archaeometry* **41**, 339-  
859 364 (1999).
- 860 63. Bøtter-Jensen, L., Mejdahl, V. Assessment of beta dose-rate using a GM multicounter  
861 system. *Int. J. Rad. Appl. Instrum. B.* **14**, 187-191 (1988).
- 862 64. Prescott, J. R., Hutton, J. T. Cosmic ray and gamma ray dosimetry for TL and ESR.  
863 *Int. J. Rad. Appl. Instrum.* **14**, 223-227 (1988).
- 864 65. Gale, S., Hoare, P. *Quaternary Sediments: Petrographic Methods for the Study of*  
865 *Unlithified Rocks* (Belhaven and Halsted Press, 1991).
- 866 66. Palmer, A. P., Lee, J. A., Kemp, R. A., Carr, S. J. *Revised laboratory procedures for*  
867 *the preparation of thin sections from unconsolidated sediments*. (Centre for  
868 micromorphology publication, Royal Holloway, University of London, 2008).
- 869 67. Kemp, R. A. *Soil micromorphology and the Quaternary*. (Quaternary Research  
870 Association, 1985).



- 871 68. Stoops, G. *Interpretation of micromorphological features of soils and regoliths*  
872 (Elsevier, 2010).
- 873 69. Rengberg, I. A procedure for preparing large sets of diatom sets from sediment. *J.*  
874 *Palaeolimnol* **4**, 87-90 (1990).
- 875 70. Battarbee, R. W., Knen, M. J. The use of electronically counter microspheres in  
876 absolute diatom analysis. *Limnol. Oceanogr.* **27**, 184-188 (1982).
- 877 71. Krammer, K., Lange-Bertalot, H. *Bacillariophyceae 2. Teil Epithemiaceae,*  
878 *Suirellaceae* (Gustav-Fisher Verlag, 1988).
- 879 72. Krammer, K., Lange-Bertalot, H. *Bacillariophyceae 3. Teil Centrales,*  
880 *Fragicariaceae, Eunotiaceae* (Gustav-Fisher Verlag, 1991a).
- 881 73. Krammer, K., Lange-Bertalot, H. *Bacillariophyceae 4. Teil Achnanthaceae, Kritsche*  
882 *Ergänzungen zu Navicula (Lineolate) und Gomphonema* (Gustav-Fisher Verlag,  
883 1991b).
- 884 74. Crawford, R. M., Likhoshway, Y. V., Jahn, R. Morphology and identity of  
885 *Aulacoseira italic* and typification of *Aulacoseira* (Bacillariophyta). *Diatom*  
886 *Research* **18**, 1-19 (2003).
- 887 75. Navok, T., Guillory, W. X., Julius, M. L., Theriort, E. C., Alverson, A. J. Towards a  
888 phylogenetic classification of species belonging to the diatom genus *Cyclotella*  
889 (Bacillariophyceae): Transfer of species formerly placed in *Puncticulata*,  
890 *Handmannia*, *Pliocaenicus* and *Cyclotella* to the genus *Lindavia*. *Phytotaxa* **217**, 249-  
891 264 (2015).
- 892 76. Ter Braak, C. J. F., Šmilauer, P. *CANOCO reference manual and CanoDraw for*  
893 *Windows user's guide: software for canonical community ordination (version 4.5).*  
894 (Microcomputer Power, 2002).

- 895 77. Hill, M. O., Gauch, H. G. Detrended correspondence analysis: An improved  
896 ordination technique. *Plant. Ecol.* **42**, 47-58 (1980).
- 897 78. Ter Braak, C. J. F., Prentice, I. C. A theory of gradient analysis. *Adv. Ecol. Res.* **18**,  
898 271-317 (1988).
- 899 79. Ter Braak, C. J. F. Canonical Correspondence Analysis: A new eigenvector technique  
900 for multivariate direct gradient analysis. *Ecology* **67**, 1167-1179 (1986).
- 901 80. Smol, J. P. et al. Climate-driven regime shifts in the biological communities of arctic  
902 lakes. *Proc. Natl. Acad. Sci. USA* **102**, 4397-4402 (2005).
- 903 81. Birks, H. J. B., Gordon, A. D. *Numerical methods in Quaternary Pollen Analysis*.  
904 (Academic Press, 1985).
- 905 82. Juggins, S. *ZONE software, version 1.2*. (University of Newcastle, 1985).
- 906 83. Bennett, K. D. Determination of the number of zones in a biostratigraphical sequence.  
907 *New Phytologist* **132**, 155-170 (1996).
- 908 84. Ryves, D. B. Juggins S., Fritz, S. C., Battarbee, R. W. Experimental diatom  
909 dissolution and the quantification of microfossil preservation in sediments.  
910 *Palaeogeogr. Palaeoclimatol. Palaeoecol.* **172**, 99-113 (2001).
- 911 85. Candy, I. et al. The evolution of Palaeolake Flixton and the environmental context of  
912 Starr Carr: an oxygen and carbon isotopic record of environmental change for the  
913 early Holocene. *Proc. Geol. Assoc.* **126**, 60-71 (2015).
- 914 86. Domínguez-Rodrigo, M., Barba, R., De la Torre, I., Mora, R. in *Deconstructing*  
915 *Olduvai: A Taphonomic Study of the Bed I Sites* (eds. Domínguez-Rodrigo, M.,  
916 Barba, R., Egeland, C. P.) 101-125 (New York, Springer, 2007).
- 917 87. Bunn, H. T. *Meat-eating and human evolution: Studies on the diet and subsistence*  
918 *patterns of Plio-Pleistocene hominids in East Africa* (University of Wisconsin,  
919 Madison, Unpublished PhD thesis, 1982).

- 920 88. Bunn, H. T., Kroll, E. M. Systematic butchery by Pilo/ Pleistocene Hominids at  
921 Olduvai Gorge , Tanzania. *Curr. Anthropol.* **27**, 431–452 (1986).
- 922 89. Binford, L. R. *Faunal remains from Klasies River Mouth.* (Academic Press, 1984).
- 923 90. Andrews, P. & Cook, J. Natural modifications to bones in a temperature setting. *Man*  
924 **20**, 675–691 (1985).
- 925 91. Blumenschine, R. J., Selvaggio, M. M. Percussion marks on bone surfaces as a new  
926 diagnostic of hominid behaviour. *Nature* **333**, 763–765 (1988).
- 927 92. Fisher, J. W. Bone Surface modifications in zooarchaeology. *J. Archaeol. Method*  
928 *Theory* **2**, 7–68 (1995).
- 929 93. Noe-Nygaard, N. Man-made trace fossils on bones. *J. Hum. Evol.* **4**, 461–461 (1989).
- 930 94. Binford, L. R. *Bones: Ancient Men and Modern Myths.* (Academic Press, 1981).
- 931 95. Stiner, M., Kuhn, S., Weiner, S., Bar-Yosef, O. Differential burning, recrystallization,  
932 and fragmentation of archaeological bone. *J. Archaeol. Sci.* **22**, 223–237 (1995).
- 933 96. Shipman, P., Foster, G., Schoeninger, M. Bunt bones and teeth: an experimental study  
934 of color, morphology, crystal structure and shrinkage. *J. Archaeol. Sci.* **11**, 307–325  
935 (1984).
- 936 97. Tong, H. W., Zhang, S., Chen, F., Li, Q. Rongements sélectifs des os par les porcs-  
937 épics et autres rongeurs : cas de la grotte Tianyuan, un site avec des restes humains  
938 fossiles récemment découvert près de Zhoukoudian (Choukoutien). *Anthropologie*  
939 **112**, 353–369 (2008).
- 940 98. Dart, R. A. Bone tools and Porcupine gnawing. *Am. Anthropol.* **60**, 715–724 (1958).
- 941 99. Behrensmeier, A. K. Taphonomic and ecological information from bone weathering.  
942 *Paleobiology* **4**, 150–162 (1978).
- 943 100. Behrensmeier, A. K., Gordon, K., Yanagi, G. T. Trampling as a cause of bone  
944 surface damage and psuedo-cutmarks. *Nature* **319**, 402–403 (1986).

- 945 101. Villa, P., Mahieu, E. Breakage pattern of human long bones. *J. Hum. Evol.* **21**,  
946 27–48 (1991).
- 947 102. Bunn, H. T. in *Animals and Archaeology, Volume 1* (eds. Clutton-Brock, J. &  
948 Grigson, C.) **1977**, 143–148 (Oxford, BAR International Series 163, 1983).
- 949 103. Scerri, E. M. L., Groucutt, H. S., Jennings, R. P., Petraglia, M. D. Unexpected  
950 technological heterogeneity in northern Arabia indicates complex Late Pleistocene  
951 demography at the gateway to Asia. *J. Hum. Evol.* **75**, 125-142 (2014).
- 952 104. Scerri, E. M. L., Gravina, B., Blinkhorn, J., Delagnes, A. Can lithic attribute  
953 analyses identify discrete reduction trajectories? A quantitative study using refitted  
954 lithic sets. *J. Arch. Method Theory* **23**, 669-691 (2016).
- 955 **105.** Groucutt, H.S., et al. Late Pleistocene lakeshore settlement in northern Arabia:  
956 Middle Palaeolithic technology from Jebel Katefeh, Jubbah. *Quatern. Int.* **382**, 215-  
957 236 (2016).